

Type Ia Supernovae Selection and Forecast of Cosmology Constraints for the Dark Energy Survey

Eda Gjergo,^{a,b} Jefferson Duggan,^c John D. Cunningham,^{c,a}
Steve Kuhlmann,^a Rahul Biswas,^a Eve Kovacs,^a
Joseph P. Bernstein,^a Harold Spinka^a

^aArgonne National Laboratory
9700 South Cass Avenue, Lemont, IL 60439, USA

^bIllinois Institute of Technology
Applied Mathematics Office, E1 Building 10 West 32nd Street, Chicago, IL 60616

^cDepartment of Physics, Loyola University Chicago
1032 W. Sheridan Road, Chicago, IL 60660

E-mail: eda.gjergo@gmail.com, jnaggud@gmail.com, jcunni6@luc.edu,
kuhlmann@anl.gov, kovacs@anl.gov, rbiswas4@gmail.com

Abstract. We present the results of a study of selection criteria to identify Type Ia supernovae photometrically in a simulated mixed sample of Type Ia supernovae and core collapse supernovae. The simulated sample is a mockup of the expected results of the Dark Energy Survey. Fits to the MLCS2k2 and SALT2 Type Ia supernova models are compared and used to help separate the Type Ia supernovae from the core collapse sample. The Dark Energy Task Force Figure of Merit (modified to include core collapse supernovae systematics) is used to discriminate among the various selection criteria. This study of varying selection cuts for Type Ia supernova candidates is the first to evaluate core collapse contamination using the Figure of Merit. Different factors that contribute to the Figure of Merit are detailed. With our analysis methods, both SALT2 and MLCS2k2 Figures of Merit improve with tighter selection cuts and higher purities, peaking at 98% purity.

Keywords: supernova, cosmology

Contents

1	Motivation	1
2	Supernova Sample Simulations	2
3	Selection Criteria and Type Ia SN models	3
3.1	Supernova Sample Signal-to-Noise Cuts	3
3.2	Type Ia Model Fit Probabilities	3
3.3	Purities and Efficiencies	5
4	Dark Energy Task Force Figure of Merit	6
4.1	Figure of Merit Calculation	6
4.2	Factors affecting the Figure of Merit	9
5	Discussion	14
A	Simulation Input Details	16
B	Supplementary Figures	18

1 Motivation

In the next decade, the number of detected Type Ia supernovae (SNIa) will increase dramatically [1, 2], surpassing the resources available for spectroscopic confirmation of each supernova (SN). This has produced an increased interest in the photometric identification of SNIa in samples including significant numbers of core collapse supernovae (SNcc). In order to improve the constraints on the accelerated expansion of the universe, discovered with SNIa in the late 1990’s [3, 4], photometric typing of supernovae (SNe) must be very robust. Two recent studies of simulated SNe have approached the subject of SN photometric identification in different ways: 1) the first, Kessler *et al.* (2010) [5], compared a wide variety of photometric-typing algorithms, but did not evaluate the impact on cosmology constraints, 2) the second, Bernstein *et al.* (2011) [1] studied the impact on cosmology in detail, but only used one photometric-typing algorithm (MLCS2k2 fit quality cuts). The analysis presented in this paper is a follow-up to Bernstein *et al.*, and incorporates several new features in the analysis.

Using tight signal-to-noise ratio (SNR) cuts and a SNIa fit quality cut (MLCS2k2 model [6]), Ref. [1] achieved a purity (SNIa/Total) above 95%. The remaining SNcc had a negligible effect on cosmology. This was achieved for the case where the redshifts of the SNe were assumed to be measured accurately in a spectroscopic follow-up of the host galaxies. In this article, we follow a similar approach but extend the analysis by studying the effects of relaxing the SNR cuts and including the SALT2 SNIa model fit quality. We use data samples simulated for the 10-field hybrid footprint of the Dark Energy

Survey¹ (DES), performed with the `SNANA` package as in Ref. [1]. We have updated the SNcc simulation inputs to reflect improved knowledge of their relative fractions and brightnesses (see section §2). We present four distinct sets of SNR cuts for both the `MLCS2k2` and `SALT2` models (using the `SALT2mu` procedure in Ref. [7] to obtain distance moduli for the `SALT2` model).² The quantity `SNRMAX` is defined to be the SNR at the measured epoch of maximum signal-to-noise in each of the four DES broadband filters used in the supernova analysis. Within a single survey strategy in terms of average observing conditions and cadence, this quantity may be used as a rough proxy for how well the supernova light curve was measured. Our goal is to find the purity levels that optimize the Dark Energy Task Force (DETF) [8] Figure of Merit (FoM). One obvious question is: What is a significant level of change in FoM? Our goal is to have the uncertainty in FoM due to the SNcc sample to be much smaller than the largest uncertainty in Ref. [1], which was due to the filter zeropoint uncertainty. The filter zeropoint uncertainty caused a 70 unit reduction in the FoM (30%). Therefore, we consider changes of >10% to be significant in our analysis. We are not considering the entire suite of systematic uncertainties in this analysis, only the impact of photometric typing and selection cuts for the mixed SNe sample.

The outline of the paper is as follows. We present the changes in the simulation of the SNcc sample in §2. Our variety of SNR selection criteria, the SNIa models we are using, and the resulting purities and efficiencies are presented in §3. The DETF Figure of Merit calculation, some relevant factors and examples, and the final results are presented in §4. We discuss the results in §5 and include more details of the new simulation inputs in Appendix A. Finally, we include supplementary figures in Appendix B.

2 Supernova Sample Simulations

The `SNANA` package [9] is used to simulate the light curves of the 5-year SNIa and SNcc samples for the DES. The simulations are very similar to those in Ref. [1] but have been updated and improved with more recent information. The list of changes since Ref. [1] are:

- The `SNANA` version was updated to v9.89b from v8.37. Our model choices were `MLCS2k2.v007` and `SALT2.LAMOPEN`.
- Four more SNcc templates (2 Ib/c and 2 IIP) are added to the 40 templates used in Ref. [1]. The templates are from the Supernova Photometric Classification Challenge [5].
- The results of Li *et al.* [10] are now used for the relative fractions of the SNcc sample, instead of those of Smartt *et al.* [11], due to a better analysis of the sample completeness.

¹<http://www.darkenergysurvey.org>

²The `SALT2` simulations used $\alpha = 0.135$ and $\beta = 3.19$. The `SALT2mu` evaluation of the distance modulus also used the same fixed values of α and β . The fitting of α and β , in the presence of significant SNcc contamination, is beyond the scope of this paper.

- The Li *et al.* [10] results are now used for the absolute brightnesses of the SNcc sample, instead of those of Richardson *et al.* [12]. This is also due to the better analysis of sample completeness.
- We now use separate relative fractions for SN Types Ib and Ic, as well as different average brightnesses based on Li *et al.*. (Type II SNe already had separate relative fractions in [1].)
- Since the Li *et al.* sample is complete, and the absolute brightnesses are not corrected for dust extinction, our simulation does not include dust extinction applied to the SNcc sample.
- The widths of the absolute brightness distributions for each type of SNcc template are matched to the measured widths from Li *et al.*

The details of these changes are available in Appendix A. The changes mostly cancel each other in terms of the overall purity of the sample with Ref. [1] cuts. The relative mixture of the SNcc sample passing cuts is more uniform, however, with less dominance from the Type Ibc SNe.

3 Selection Criteria and Type Ia SN models

3.1 Supernova Sample Signal-to-Noise Cuts

As mentioned previously, our SNR is defined at the measured epoch of maximum SNR in each filter (SNRMAX). We present four distinct sets of SNR cuts for both the MLCS2k2 and SALT2 models. For simplicity, we define the symbols used in the rest of the paper for these four sets of cuts in Tab. 1.

Cuts	Symbol
2 filters with $\text{SNRMAX} \geq 3$	SNR-3-3-0
2 filters with $\text{SNRMAX} \geq 5$	SNR-5-5-0
3 filters with $\text{SNRMAX} \geq 5$	SNR-5-5-5
1 filter $\text{SNRMAX} \geq 10$, 2 more filters $\text{SNRMAX} \geq 5$	SNR-10-5-5

Table 1. These are the definitions of the signal-to-noise cut symbols used throughout this work. For the first two cuts listed in the table, we removed SNe for which the third filter was less than zero. For the remainder of the paper when we refer to the “tightest” and “loosest” SNR cuts we mean SNR-10-5-5 and SNR-3-3-0 respectively.

3.2 Type Ia Model Fit Probabilities

Core collapse SNe light curves fit to a SNIa light curve model might be expected to have bad fit qualities, and this was demonstrated in Ref. [1]. Motivated by this, we reject SN candidates which have deviations from the best fit light curve model (whether MLCS2k2 or SALT2) that are statistically large compared to the errors. This is quantified

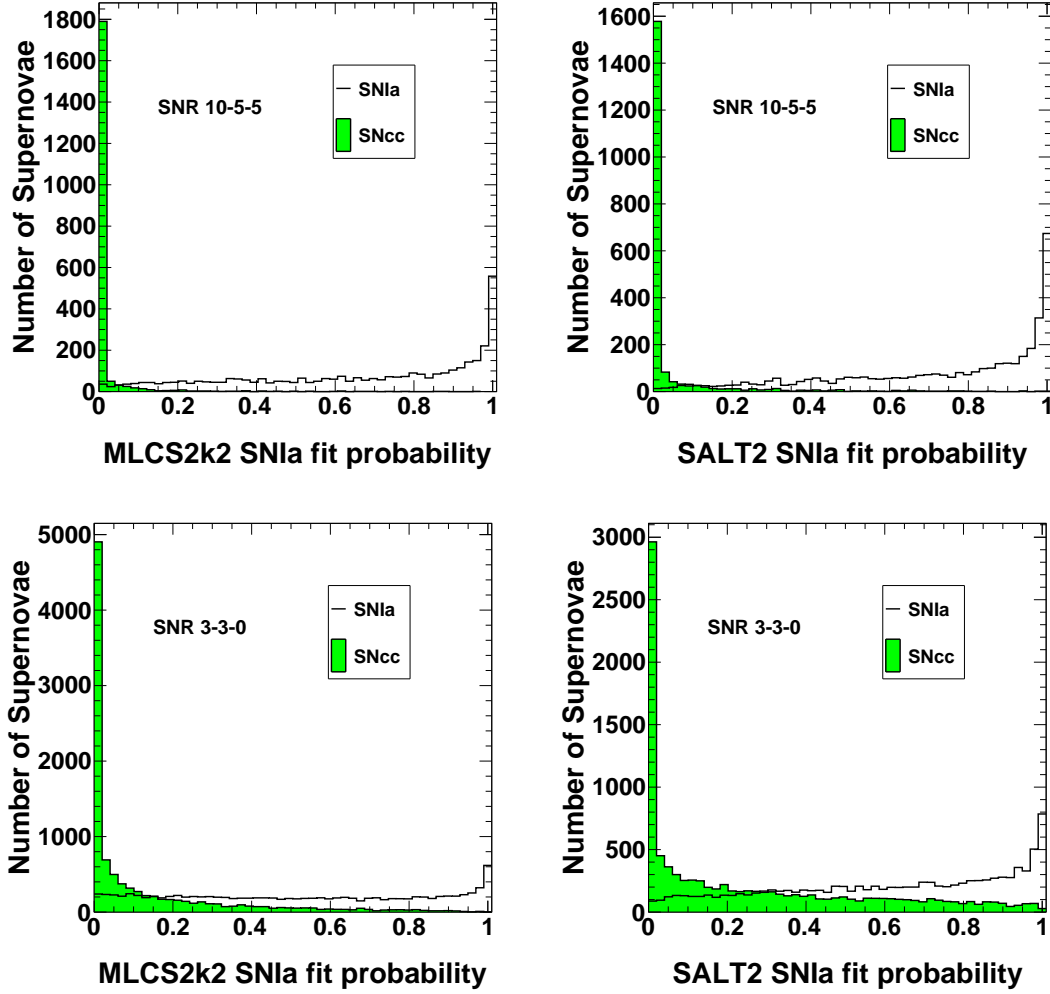


Figure 1. The MLCS2k2 fit probabilities (*left panels*) are plotted for the SNIa and SNcc samples. The top left panel is for the tightest SNR cuts, SNR-10-5-5, while the bottom left panel is for the loosest SNR cuts, SNR-3-3-0. The corresponding SALT2 fit probabilities are shown in the right panels, with the tightest cuts on top and the loosest cuts on bottom.

in terms of fit probabilities³ obtained from the light-curve χ^2 and the number of degrees of freedom. Figure 1 shows the results of the fit probabilities for both models, and for our tightest and loosest cuts. It is evident that the SALT2 model has larger fit probabilities for the SNcc sample and hence we obtain lower purities for SALT2 compared to those of MLCS2k2. This is most likely due to the use of tight dust extinction priors used in the

³If the observed deviations from the best fit model were due to Gaussian fluctuations compatible with the reported errors on observations, this is the probability of the χ^2 being larger than the observed χ^2 for the number of degrees of freedom in the light curve fit.

MLCS2k2 fits [1]. But as described in Ref. [1], these MLCS2k2 priors lead to additional SNe color systematics not present in SALT2 fits.

3.3 Purities and Efficiencies

In this section, we present the results for purities and SNIa efficiencies for the four sets of SNRMAX cuts and with the MLCS2k2 and SALT2 fit probability cuts described above. We define the SNIa efficiency as the ratio of the number of SNIa passing all cuts that define the sample to the total number of SNIa simulated. For our calculation of efficiency, the denominator is the complete sample of SNIa generated with zero SNR cuts and the rates described in Ref. [1]. Many studies of SNIa efficiencies apply different sets of base SNR cuts, making it difficult to compare efficiencies from different analyses. We define the sample purity as the ratio of the number of SNIa to the total number of SNIa+SNcc passing all cuts. The numbers of SNIa and SNcc and the related purities and efficiencies integrated over all redshifts are presented in Tab. 2. Figure 2 shows the purities and efficiencies as functions of redshift for the tightest and loosest SNR cuts for both the MLCS2k2 and SALT2 models. As discussed above for Fig. 1, the SALT2 model without tight priors is more flexible and leads to lower purities than our current implementation of the MLCS2k2 model.

SNRMAX Cuts	Algorithm	SNIa	SNcc	Purity	Efficiency
SNR-10-5-5	$f_p\text{MLCS} > 0.1$	3534	88	98%	20%
SNR-5-5-5	$f_p\text{MLCS} > 0.1$	4659	240	95%	27%
SNR-5-5-0	$f_p\text{MLCS} > 0.1$	5949	534	92%	34%
SNR-3-3-0	$f_p\text{MLCS} > 0.1$	9206	3138	75%	53%
SNR-10-5-5	$f_p\text{SALT} > 0.1$	3686	236	94%	21%
SNR-5-5-5	$f_p\text{SALT} > 0.1$	4820	568	89%	27%
SNR-5-5-0	$f_p\text{SALT} > 0.1$	6425	1173	85%	37%
SNR-3-3-0	$f_p\text{SALT} > 0.1$	9776	5298	65%	56%

Table 2. The simulated SNe sample purities and efficiencies are presented for a variety of selection criteria (symbols defined in Tab. 1) and two SNIa identification methods ($f_p\text{MLCS}$ and $f_p\text{SALT}$ are the fit probabilities for the MLCS2k2 and SALT2 models respectively). For the calculation of efficiency, the denominator is the complete sample of SNIa generated with no SNR cuts. The number of input SNIa was 17555.

Figure 3 shows some characteristics of the SNIa and SNcc samples that pass the fit probability cuts. The SNIa redshift distributions shown on the top panel demonstrate the increasing SNIa efficiency at large redshift as the cuts are relaxed. The top left panel is for MLCS2k2 and the top right panel is for the SALT2 model. The Hubble scatter shown on the lower panels is for the SNcc sample passing the SNR-10-5-5 cuts and a fit probability > 0.1 cut in each case. The number of type IIL SNcc is significantly more than in Ref. [1]. The numbers for each SNcc type with the SNR-10-5-5 cuts are shown in Tab. 3. This change in SNcc numbers is due to the simulation input changes described in §2 and Appendix A.

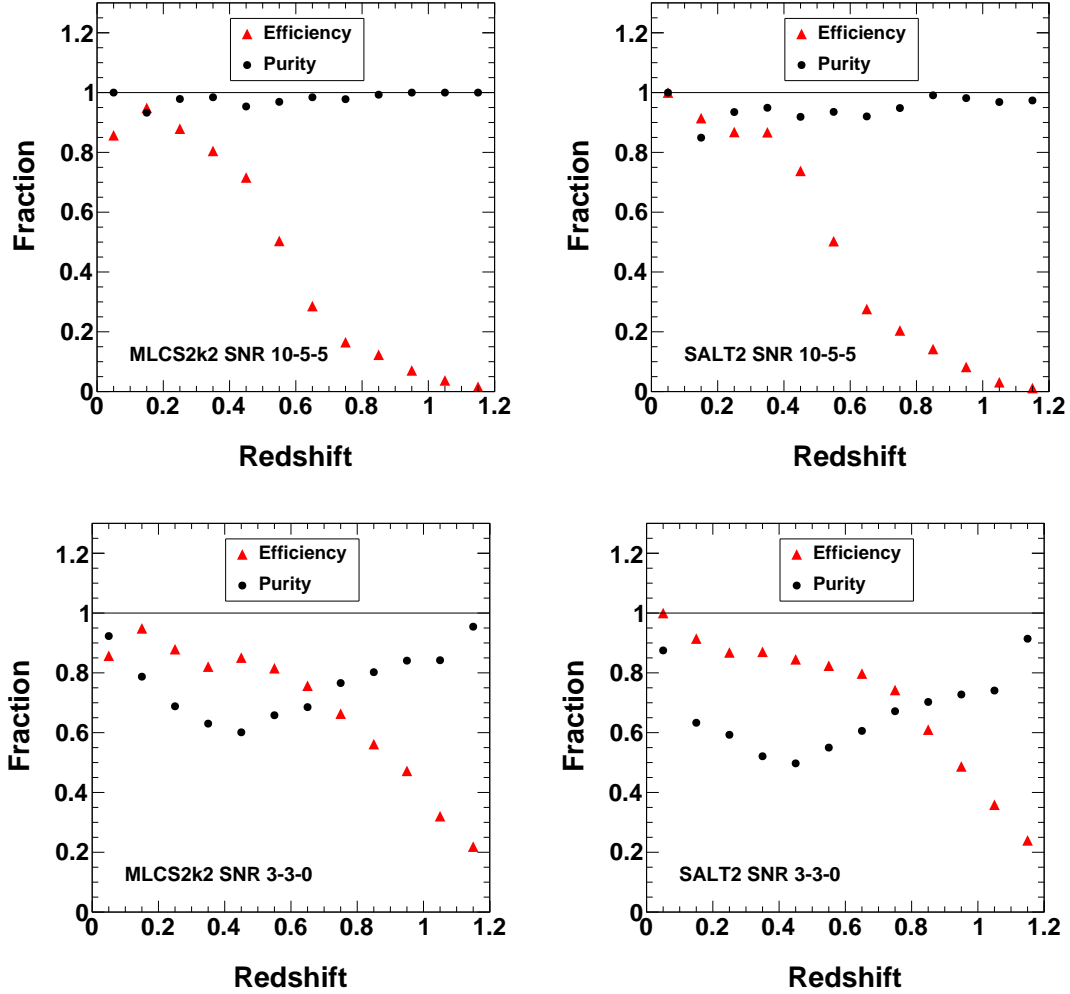


Figure 2. The MLCS2k2 purities and SNIa efficiencies are plotted in the left panels. The definition of SNIa efficiency is the same as in Tab. 2. The top left panel is for the tightest SNR cuts, SNR-10-5-5, while the bottom left panel is for the loosest set of SNR cuts, SNR-3-3-0. The corresponding SALT2 purities and SNIa efficiencies are shown in the right panels, with the tightest cuts on top and the loosest cuts on bottom. The jumps in purity observed at some redshifts are due to low statistics in the SNcc passing the cuts.

4 Dark Energy Task Force Figure of Merit

4.1 Figure of Merit Calculation

As described in Ref. [1], constraints on cosmological parameters are obtained by comparing the predicted theoretical values of distance moduli, $\mu(z, \theta_c)$, to the values inferred from the light curve fits of the SN simulations, $\mu_{obs}(z)$, where: $\theta_c \equiv \{\Omega_{DE}, w_0, w_a, \Omega_k\}$

Type	Bernstein <i>et al.</i>	This Analysis
Ib/c	57	54
IIP	2	5
IIn	2	0
IIL	2	29

Table 3. The number of core collapse supernovae passing the tightest SNR-10-5-5 cuts and $f_p\text{MLCS} > 0.1$, compared to Ref. [1]. The large increase in the number of Type IIL SNe passing cuts is mostly due to the 0.5 magnitude brighter input value to the *SNANA* template, coming from Ref. [10].

is the set of cosmological parameters. Here, Ω_{DE} and Ω_k are the current energy densities corresponding to Dark Energy and spatial curvature as a fraction of the critical density. The parameters w_0, w_a are the parameters in a CPL parametrization [13, 14] of the equation of state: $w(a) = w_0 + w_a(1 - a)$. The likelihood for an individual SN, at redshift z_i , is taken to be a Gaussian with a mean given by the $\mu(z_i, \theta_c)$ at redshift z_i for the cosmological parameters θ_c . The simulated SN observations are independent and the likelihood is analytically marginalized over the nuisance-parameter combination of the Hubble Constant, H_0 , and the absolute magnitude, M , with a flat prior on M . Following the DETF Report [8], we evaluated the performance of photometric identification algorithms and selection criteria in terms of the DETF FoM.

The distance modulus errors used in the FoM calculation are typically derived from the light curve fit errors and an intrinsic dispersion $\sigma_{int} = 0.13$ added in quadrature as in Ref. [1]. For a pure SNIa sample, the intrinsic dispersion is chosen to give $\chi^2/DOF \sim 1$ (DOF=number of degrees of freedom) in the cosmology fit. This procedure works for a very pure sample but will fail to account for the additional dispersion due to SNcc contamination. Therefore, we will take an additional step in this analysis of determining the RMS of the total SNIa+SNcc sample in each of 12 redshift bins. We then inflate the input errors for the FoM calculation by adding an additional amount in quadrature to the reported errors such that the means of the inflated errors match those RMS values. This ensures a reasonable $\chi^2/DOF \sim 1$ in the cosmology fit. Whenever we use inflated errors in the FoM calculation we do not include the 0.13 intrinsic dispersion.

We model the issue of core collapse contamination in the Figure of Merit calculation in a way similar to the method used in Ref. [1]. We assume that the distance modulus obtained by fitting a core collapse supernova to a Ia model is given by

$$\mu_{cc}(\theta_c, z) = \mu(\theta_c, z) + \eta(z)$$

where $\mu(\theta_c, z)$ is the distance modulus and $\eta(z)$ encodes the differences in characteristics of core-collapse supernovae from SNIa and is independent of the cosmology. We expect $\eta(z)$ to be different for each core-collapse supernova (certainly core collapse supernova types and templates), and hence there will be a large scatter in this quantity. For a DES simulation with a fixed set of selection cuts, we expect that $\langle \eta(z) \rangle$, the average value of $\eta(z)$ in each z bin, to be roughly consistent between different realizations of simulations.

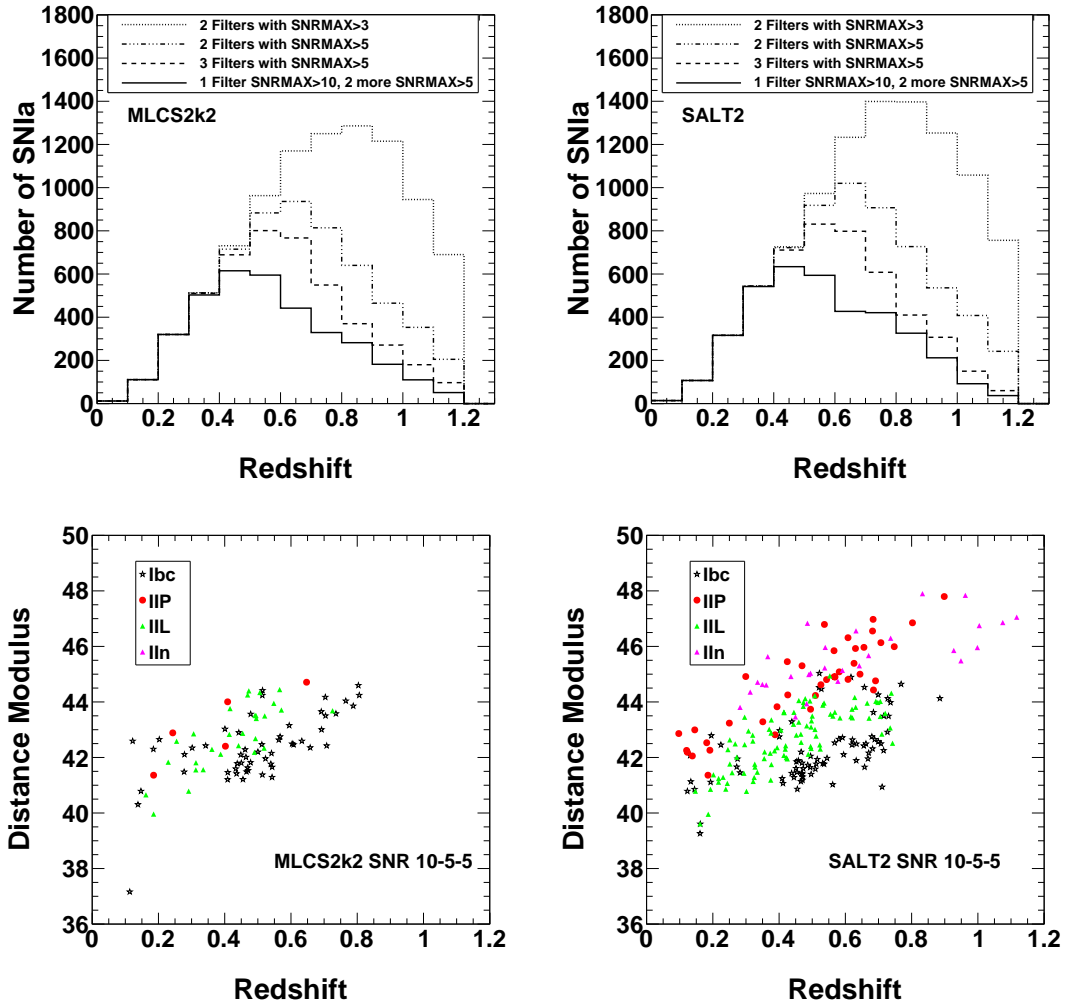


Figure 3. The top panels show the SNIa redshift distributions for the MLCS2k2 model (left) and the SALT2 model (right) for each SNRMAX cut and a fit probability > 0.1 cut in each case. The lower panels show the Hubble scatter for the SNcc sample passing the tightest SNR-10-5-5 cut and a fit probability > 0.1 cut in each case.

We use our simulated data to determine $\langle \eta(z) \rangle$ for each set of selection cuts used in this analysis.

With this information from simulations, we obtain an average correction as a function of redshift for the average shift in $\mu_{obs}(z)$ introduced by the core-collapse contamination. We parametrize this correction by noting that for a mixed sample the average

value of $\mu_{obs}(z)$ is given by

$$\begin{aligned}\langle\mu_{obs}\rangle &= f(z)\langle\mu_{cc}\rangle + (1 - f(z))\langle\mu_{Ia}\rangle, \\ &= \mu(\theta_c, z) + f_{cc} [F(z)\langle\eta(z)\rangle],\end{aligned}\tag{4.1}$$

where $f(z)$ is the probability that a randomly selected supernova at redshift z in the mixed sample is a core collapse supernova, $f_{cc} = 1 - \text{purity}$, $F(z) = f(z)/f_{cc}$, and we have assumed that the observed distance moduli of SNIa are unbiased estimates of the distance moduli $\mu(\theta_c, z)$. The average correction is the second term in Eqn. 4.1 and the part in the square brackets is computed from simulations and is held fixed. Thus, we expand our set of model parameters to include f_{cc} and study joint constraints on all the parameters including f_{cc} . In order to obtain a Figure of Merit analogous to the DETF FoM, we evaluate a Fisher Matrix at the DETF fiducial values of the cosmological parameters and marginalize over all parameters other than w_0 and w_a . In doing so, we use priors on the model parameters. A Gaussian prior on f_{cc} with a standard deviation assumed to be equal to f_{cc} is used. The choices of priors on cosmological parameters are the same as those used in Ref. [1]: a Fisher matrix representing priors on the set of cosmological parameters from DETF StageII experiments and expected Planck data was used along with a set of low redshift supernovae from experiments that were not included in calculating the StageII Fisher matrix mentioned above. These low redshift SNe were spectroscopically identified, and thus neither of the modifications for core-collapse supernovae (the inflation of the reported errors to match RMS or the use of the polynomial) were applied to these supernovae.

4.2 Factors affecting the Figure of Merit

In this section, we investigate various factors that affect the DETF Figure of Merit, and give a step-by-step example of how the FoM changes with each factor. We first investigate our sensitivity to the fit probability cut shown in Fig. 1. We show in Tab. 4 how the FoM changes for fit probabilities greater than 0.05, 0.1 and 0.2, for the tightest (SNR-10-5-5) and loosest (SNR-3-3-0) cuts. The FoM is relatively insensitive to the precise fit probability cut for both MLCS2k2 and SALT2. Therefore for the rest of this paper, we will use 0.1 as the cut point, the same as in Ref. [1].

We now investigate four factors that significantly affect the DETF Figure of Merit:

- the number of SNIa (N_{Ia}),
- the reported errors on the distance modulus,
- the effect of the additional Hubble scatter due to SNcc, which is usually much larger than the reported errors on the distance modulus,
- the uncertainty in the Hubble residual due to SNcc systematics.

The number of SNe in the sample is an obvious factor to consider. First, let us consider the simple DETF FoM without any of our modifications. Here, adding supernovae to a

SNRMAX cuts	ID algorithm	FoM SNIa+SNcc+Sys.
SNR-10-5-5	$f_p\text{MLCS} > 0.05$	189
SNR-10-5-5	$f_p\text{MLCS} > 0.1$	196
SNR-10-5-5	$f_p\text{MLCS} > 0.2$	198
SNR-3-3-0	$f_p\text{MLCS} > 0.05$	159
SNR-3-3-0	$f_p\text{MLCS} > 0.1$	158
SNR-3-3-0	$f_p\text{MLCS} > 0.2$	155
SNR-10-5-5	$f_p\text{SALT} > 0.05$	132
SNR-10-5-5	$f_p\text{SALT} > 0.1$	132
SNR-10-5-5	$f_p\text{SALT} > 0.2$	140
SNR-3-3-0	$f_p\text{SALT} > 0.05$	105
SNR-3-3-0	$f_p\text{SALT} > 0.1$	104
SNR-3-3-0	$f_p\text{SALT} > 0.2$	103

Table 4. The DETF Figure of Merit, including SNcc systematics, is presented for a variety of MLCS2k2 and SALT2 fit probability selection criteria and for the loosest and tightest cuts considered and found to be relatively insensitive to exact value of the fit probability thresholds.

sample will always improve the FoM. If the supernovae added have the same statistical properties (similar error bars) then the rate of improvement with numbers depends on the priors used in the calculation. This dependence can be observed in the left panel of Fig. 4, where independent statistically equivalent samples of SNIa passing selection cuts SNR-10-5-5 (such as would be obtained by using more seasons of DES observation using the same selection cuts) have been added. The lower curve, approximately linear⁴, is the variation of the FoM with no DETF Stage II or Planck priors, and it has been multiplied by 1000 in order to be visible. That demonstrates how critically important the priors are in the FoM. The upper curve includes the DETF stage II and Planck priors and has a $\sqrt{N_{Ia}}$ dependence⁵.

We begin our step-by-step example of FoM changes with the top row of Tab. 5, for the loosest cuts SNR-3-3-0 and $f_p\text{MLCS} > 0.1$. While 9206 SNIa pass these cuts, these SNIa are not statistically equivalent to the SNIa used in the left panel of Fig. 4, as supernovae that fail the tightest cuts have larger errors on the distance modulus. The FoM value (with priors) of 310 is for the 9206 SNIa that pass these cuts with the reported distance moduli errors added in quadrature with 0.13, as discussed above, and used in Ref. [1]. The value extrapolated from the left panel of Fig. 4 is 316. The difference is even starker for second row of the table, where the FoM=354 is the extrapolated value from the left panel when the number of SN is raised to 12344, the total number of supernovae (SNIa and SNcc) in the sample. The third row of the table shows the calculated FoM of 316 using 0.13 added in quadrature to the reported distance moduli errors. Most of

⁴The linear dependence on N_{Ia} can be understood from the fact that the DETF FoM is inversely proportional to the product of errors on w_0 and w_a , each of which fall like $\sqrt{N_{Ia}}$.

⁵This dependence is difficult to predict due to the complicated effects of the priors.

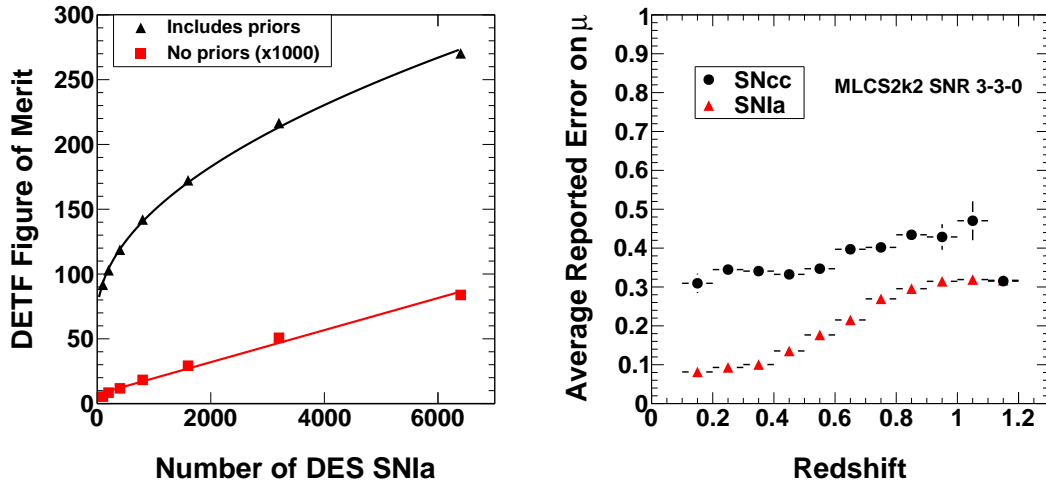


Figure 4. The Figure of Merit dependence on the number of Type Ia SNe with and without DETF Stage II and Planck priors is shown in the left panel. Note that the points without priors are multiplied by 1000. The average μ error, as reported by the MLCS2k2 Type Ia model fit, is shown for the SNIa and SNcc samples in the right panel. Note that the highest redshift point in the right panel has fluctuated so that the SNcc and SNIa points overlap and the SNIa point is not visible.

the difference between 354 and 316 is due to the reported errors on the distance moduli of SNcc being larger than SNIa, as shown in the right panel of Fig. 4.

The third factor affecting the FoM is the effect of the SNcc scatter on the Hubble diagram, demonstrated in Fig. 5 for the loosest and tightest SNR cuts for both MLCS2k2 and SALT2 models. As discussed earlier, we inflate the SNIa and SNcc input errors to the FoM determination in order to achieve a reasonable χ^2/DOF . The additional error added, for the loosest SNR-3-3-0 cuts, varies from 0.8-1.5 mags for SALT2 and 0.3-1.3 mags for the MLCS2k2 model. Our choice of the loosest SNR cuts and MLCS2k2 for our example shows the most dramatic effect of these additional errors in the fourth row of Tab. 5. This shows the FoM decreasing from 316 to 181. Note that this is just an exercise to understand the FoM better. We do not expect anyone to attempt to do a cosmology analysis with the SNcc contamination shown in Fig. 5 with the loosest cuts.

The fourth and final SNcc-related factor we consider that affects the FoM significantly is the strength of SNcc contamination. As discussed above and in Ref. [1], we model as a function of z , the change of the Hubble residual due to varying amounts of SNcc contamination, and take 100% of this change as the one standard deviation uncertainty. Figure 6 shows the change in Hubble residual due to the SNcc sample for the loosest cuts and for the MLCS2k2 and SALT2 models. The bottom row of Tab. 5 shows the FoM decreasing from 181 to 158 using the change in Hubble residual with MLCS2k2 and the loosest cuts.

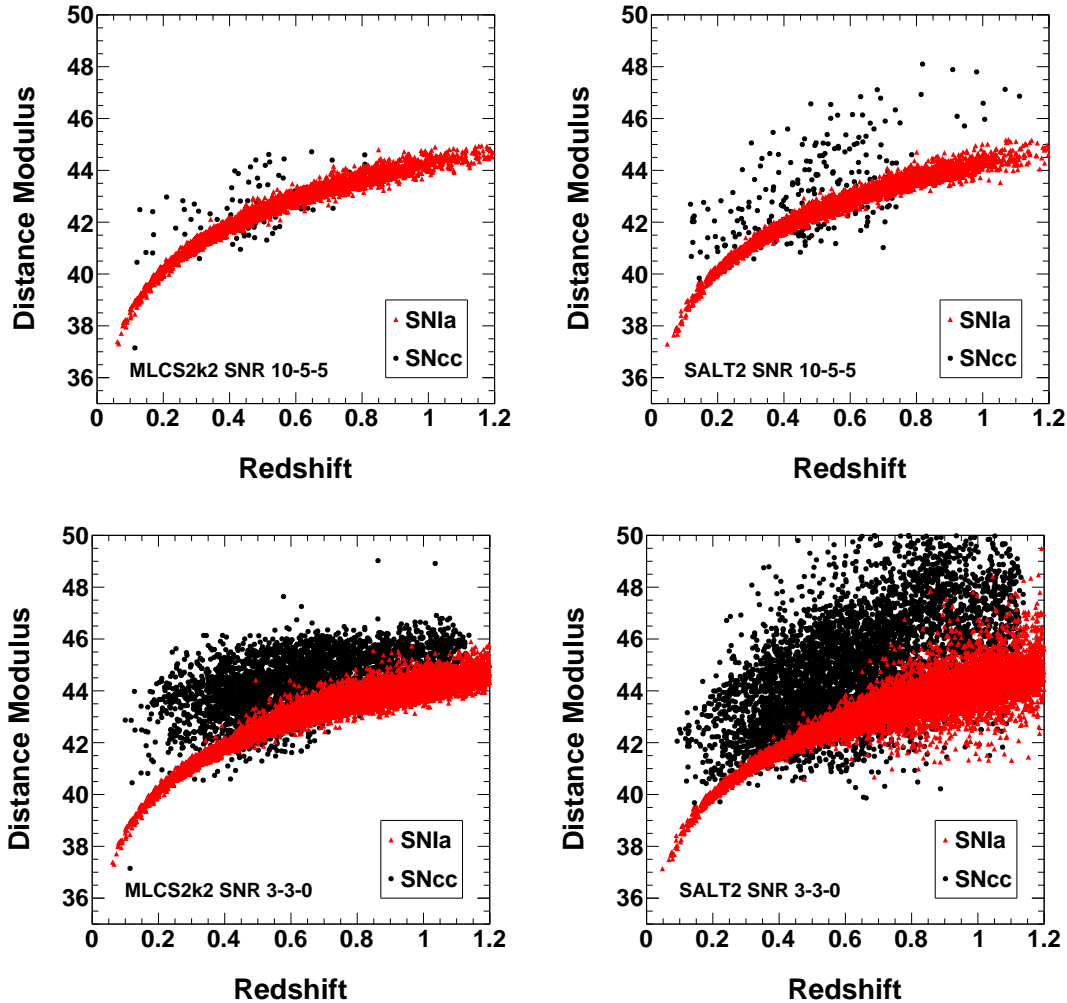


Figure 5. We display four Hubble diagrams, for both SNIa and SNcc. The top panels are for the tightest SNR-10-5-5 cuts, while the lower panels are for the loosest SNR-3-3-0 cuts. The left panels are with the MLCS2k2 light-curve fitter, while the right panels are for the SALT2 light-curve fitter. (See text for discussion.)

Table 6 shows a summary of our results, combining the four factors that affect the FoM discussed above. We present different values for the FoM, from tighter cuts (SNR-10-5-5) to looser cuts (SNR-3-3-0), for both MLCS2k2 and SALT2 models. The column labeled FoM Ia is for SNIa and incorporates the reported SNIa μ errors added to 0.13 in quadrature. The column labeled FoM Ia+CC adds the SNcc sample and includes the inflated error to make $\chi^2/DOF \sim 1$ for each sample. The final column adds the SNcc systematic described above and is the most relevant column. The FoM is best for the tightest cuts for both SALT2 and MLCS2k2 models. SNR cuts tighter than SNR-10-5-5

FoM for Ia only	310
FoM for SNIa + SNcc (Extrapolating using $\sqrt{N_{Ia}}$ dependence)	354
FoM for SNIa + SNcc(using fitter reported SNe μ error + 0.13 intrinsic dispersion)	316
FoM for SNIa + SNcc(inflated error for $\chi^2/DOF \sim 1$)	181
FoM for SNIa + SNcc(inflated error for $\chi^2/DOF \sim 1$ and SNcc systematic)	158

Table 5. The most important factors that can change the DETF Figure of Merit are demonstrated with an example for MLCS2k2. (See the text for a detailed discussion.)

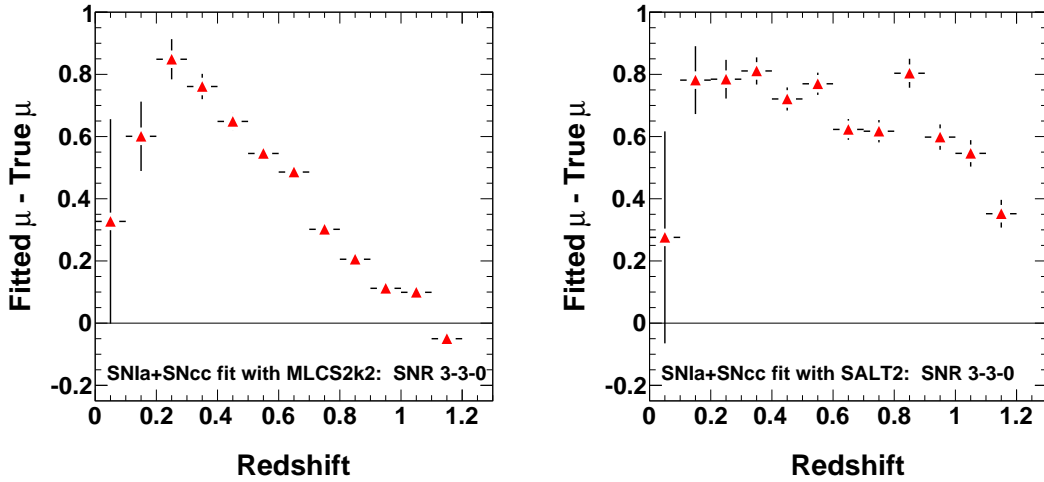


Figure 6. The Hubble residual is shown when the core collapse sample is included, for the MLCS2k2 Type Ia model on the left and the SALT2 model on the right, both with the loosest SNR-3-3-0 cuts.

were also analyzed. It is expected that as the SNR cuts are tightened, and purities approach 100%, the loss in SNIa statistics will cause a drop in FoM. We observe this for both MLCS2k2 and SALT2, but at different SNR cut values in each case. However, for both MLCS2k2 and SALT2, the peak FoM value occurred at 98% purity (SNR-10-10-5 and SNR-10-5-5 had almost identical purity and FoM for MLCS2k2 and SNR-10-10-10 had the peak FoM for SALT2).

We observe again that the SALT2 fitter allows more SNcc into our sample than MLCS2k2 and results in lower purities for a given set of SNR cuts. In addition, the Hubble scatter for the SNcc is larger for SALT2 than MLCS2k2. The lower purity and larger scatter cause lower FoM for the samples fit with the SALT2 model. As mentioned earlier, this is at least partly due to the tight dust extinction priors used in the MLCS2k2 fits [1].

SNRMAX cuts	SN Ia ID	SN Ia	Pur.	FoM Ia	FoM Ia+CC	FoM Ia+CC+Sys.
SNR-10-5-5	f_p MLCS > 0.1	3534	98%	249	203	196
SNR-5-5-5	f_p MLCS > 0.1	4659	95%	266	200	172
SNR-5-5-0	f_p MLCS > 0.1	5949	92%	285	197	167
SNR-3-3-0	f_p MLCS > 0.1	9206	75%	310	181	158
SNR-10-5-5	f_p SALT > 0.1	3686	94%	234	147	132
SNR-5-5-5	f_p SALT > 0.1	4820	89%	246	151	131
SNR-5-5-0	f_p SALT > 0.1	6425	85%	263	144	120
SNR-3-3-0	f_p SALT > 0.1	9776	65%	276	130	104

Table 6. The Dark Energy Task Force Figure of Merit is presented for a variety of selection criteria (symbols defined in Tab. 1) and fits to two SN Ia models. The columns, from left to right, are: cut value, SN Ia model used, number of SN Ia passing all cuts, purity of the sample, the FoM for a SN Ia-only sample and statistical uncertainties only, the FoM for the combined SN Ia+SNcc sample using the inflated errors for the complete sample, and the FoM for the combined sample including the core collapse systematic uncertainty. SNRMAX cuts tighter than those shown in this table were investigated. For both MLCS2k2 and SALT2, the FoM decreased for purities higher than 98%.

5 Discussion

This analysis is an extension of the Bernstein *et al.* [1] paper with a focus on the Type Ia/core collapse separation. The previous analysis used one set of SNR cuts and one SN Ia identification model and found a negligible effect on cosmology. On the other hand, the tight cuts led to a low efficiency for SN Ia. It is natural to investigate additional SNR cuts and models.

The main extensions to Ref. [1] addressed in this analysis are listed below:

- four sets of SNR cuts are used instead of one,
- the MLCS2k2 and SALT2 models are treated on equal footing,
- the SNANA simulation inputs for core collapse simulations have been updated with more current knowledge (a total of seven input changes were made and are detailed in Appendix A),
- a variety of fit probability and purity/efficiency plots are presented,
- a detailed purity and efficiency table for all variations is presented,
- the Dark Energy Task Force Figure of Merit is tested on all variations,
- the normal procedure of adding an intrinsic dispersion ~ 0.13 in quadrature with the reported μ error is supplemented by a new procedure that uses inflated errors determined from the Hubble diagram RMS of the total SN Ia+SNcc sample in redshift bins,

- other significant factors in the FoM are examined, such as the scaling with number of supernovae and large impact of the DETF stage II and Planck priors (more than x1000 increase in FoM), as well as the core collapse systematic uncertainty.

The changes to the simulation inputs caused very little change in resulting purities, compared to Ref. [1]. The most significant change is in the Type IIL simulation, which increased in number passing cuts by almost a factor of 15. This is mostly due to the 0.5 magnitude brighter input value to the SNANA template, coming from Ref. [10]. This highlights a fragility in the current knowledge of core collapse simulations, there is only one Type IIL template available to generate the simulations. Hopefully this can be supplemented by more templates in the future.

We find the SALT2 model allows more SNcc passing the fit probability cuts compared to the MLCS2k2 model (which includes dust extinction priors) and leads to somewhat lower purities and lower FoM. The scatter in the SNcc μ values is also larger for the SALT2 model, and this also contributes to lower FoM with our treatment of core collapse uncertainties. The more significant result, however, is that for both models the FoM decreases with purities lower than 98%. Purities higher than 98% were analyzed and the FoM decreased for both models due to a loss of SNIa statistics.

This analysis lays the groundwork for future analyses of more sophisticated photometric types [5], as well as the application of additional cuts, such as SNe color and stretch. From the top panels in Fig. 3, it is clear that the SNIa sample is complete up to $z \sim 0.4$ even with the tightest SNR cuts. Therefore, loosening SNR cuts for low redshift only increases the SNcc contamination. Furthermore, at $z \gtrsim 0.8$ the purity is increasing even with the loosest cuts. These trends imply that using a z -dependent SNR cut would be a better choice.

In addition, it is obvious from the Hubble scatter plots that many of the SNcc are easily removed, as their μ values are many standard deviations away from any possible cosmology. Coupled with potential μ cuts, it is necessary to study fitted cosmology biases for each possible sample, since the DETF FoM is not sensitive to these biases. Another challenging future study is the measurement of SNe colors (either SALT2 β or MLCS2k2 R_V), as a function of redshift, in the presence of varying amounts of SNcc contamination. Finally, the treatment of the core collapse systematic (100% of the shift in Hubble residual) is simplistic and can be improved with a breakdown of the individual components of the core collapse uncertainties.

Acknowledgments

We thank Rick Kessler for his advice concerning the SNANA simulations used in this paper. We thank Kyler Kuehn for a critical reading of the manuscript.

The submitted manuscript has been created by UChicago Argonne, LLC, Operator of Argonne National Laboratory (“Argonne”). Argonne, a U.S. Department of Energy Office of Science laboratory, is operated under Contract No. DE-AC02-06CH11357. The U.S. Government retains for itself, and others acting on its behalf, a paid-up nonexclusive, irrevocable worldwide license in said article to reproduce, prepare derivative works,

distribute copies to the public, and perform publicly and display publicly, by or on behalf of the Government.

A Simulation Input Details

In §2 we listed seven improvements to the core collapse simulations, implemented since Ref. [1]. In this appendix, we provide more details for the experts in the field that are interested in reproducing or expanding upon our simulations.

Measurements of the relative fractions of SNcc have improved recently, largely due to the LOSS data presented in Ref. [10]. Table 7 compares the relative fractions of SNcc between Smartt *et al.* [11] and Li *et al.* [10].

SNe Type	Smartt <i>et al.</i> %	Li <i>et al.</i> %
Ib	9.8	5.2
Ic	19.6	13.3
Ibc-pec	N/A	6.0
II-P	58.7	52.7
II-L	2.7	7.3
IIb	5.4	9.0
IIc	3.8	6.5

Table 7. Comparison of core collapse relative fractions from Smartt *et al.* [11] and Li *et al.* [10].

We have made modifications in these relative SNcc fractions for our analysis since the Bernstein *et al.* paper:

- we use the Li *et al.* fractions with their inherent higher statistics and better sample completeness instead of the Smartt *et al.* fractions,
- for the Type Ib and Ic fractions, we take half of the total Ibc-pec (6%) fraction and add this percentage (3%) to each of the Ib and Ic fractions (This is justified since Li *et al.* reported that the photometric behaviors of these SN Ibc-pec are all reasonably represented by the average SN Ibc light curve.),
- we combine the II-L and IIb samples ($7.3\% + 9.0\% = 16.3\%$), since there are no IIc templates available currently in the SNANA package.

The input relative fractions to SNANA are summarized in Table 8.

The uncertainties in the absolute brightnesses of SNcc are greater than the uncertainties in the relative fractions. The absolute brightnesses can dramatically affect the number of SNcc passing various selection cuts. We have also made a change in the input parameters of SNANA for the absolute brightnesses. Instead of the Richardson *et al.* [12] brightnesses (corrected in an ad hoc way for Malmquist bias), we use the Li *et al.* brightnesses. Table 9 compares the absolute brightnesses and widths presented in Li *et al.* and Richardson *et al.* One important aspect to note is that the Richardson *et al.*

SNe Type	Li <i>et al.</i> (%)	Input to SNANA(%)
Ib	5.2	8.2
Ic	13.3	16.3
Ibc-pec	6.0	0
II-P	52.7	52.7
II-L	7.3	16.3
IIb	9.0	0
IIn	6.5	6.5

Table 8. We show a comparison of core collapse relative fractions from Li *et al.* [10] and those input to SNANA.

and Li *et al.* absolute brightnesses are in the B-band and R-band, respectively. Since the Li *et al.* measured widths are broader than those of Richardson *et al.*, we have added additional smearing to the input SNcc templates in the SNANA simulation. A comparison of simulation-template magnitude offsets between Richardson *et al.* and Li *et al.* is presented in Tab. 10 (i.e. Simulated Template Peak Brightness = Measured Template Peak Brightness + Mag. Offset). After the magnitude offset is added, an additional gaussian brightness smearing is applied with the one standard deviation values also presented in Tab. 10. The net effect of these changes is to ensure that the SNcc template-brightness mean and RMS used in SNANA match the results of Li *et al.*.

SNe Type	$M_B(\text{Rich.})$	$\sigma_{M_B}(\text{Rich.})$	$M_R(\text{Li})$	$\sigma_{M_R}(\text{Li})$
IP	-14.40 ± 0.42	0.81	-15.66 ± 0.16	1.23
Ib/c	-16.72 ± 0.23	0.62	-16.09 ± 0.23	1.24
II-L	-17.19 ± 0.15	0.47	-17.44 ± 0.22	0.64
IIn	-17.78 ± 0.41	0.74	-16.86 ± 0.59	1.61

Table 9. We present a comparison of means and RMS of the SNcc absolute-brightness distributions from Richardson *et al.* [12] (B-band) and Li *et al.* [10] (R-band).

SNe Type	Mag. Offset (Rich.)	Mag. Smearing (Rich.)	Mag. Offset (Li)	Mag. Smearing (Li)
Ib/c	0.25	0.000	0.0	0.0
Ib	0.00	0.000	0.5	0.1
Ic	0.00	0.000	1.4	1.2
IIn	0.00	0.742	1.0	1.5
II-P	1.87	0.000	2.1	1.1
II-L	-0.30	0.469	-0.80	0.6

Table 10. We show a comparison of core collapse SNANA magnitude offsets and magnitude smearing from Richardson *et al.* [12] (B-band) and Li *et al.* [10].(R-band).

B Supplementary Figures

In this appendix we present several supplementary figures; each one is meant to complete the set of SNR cuts shown in plots earlier in the paper. The figure captions should be self-explanatory.

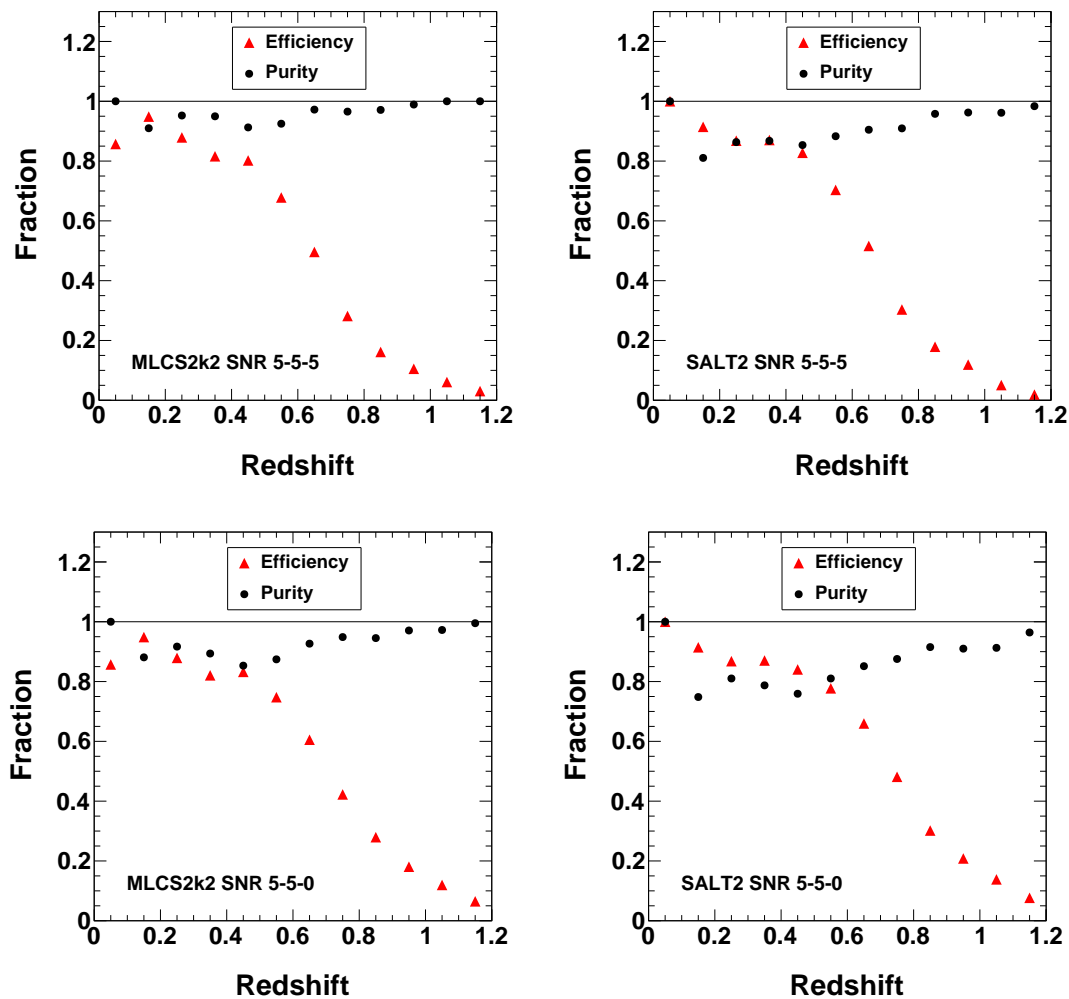


Figure 7. As in Fig. 2, the MLCS2k2 purities and SNIa efficiencies (*left panels*) are plotted. The definition of SNIa efficiency is the same as in Tab. 2. The top left panel is for the SNR cuts SNR-5-5-5, while the bottom left panel is for the SNR cuts SNR-5-5-0. The corresponding SALT2 purities and SNIa efficiencies are shown in the right panels.

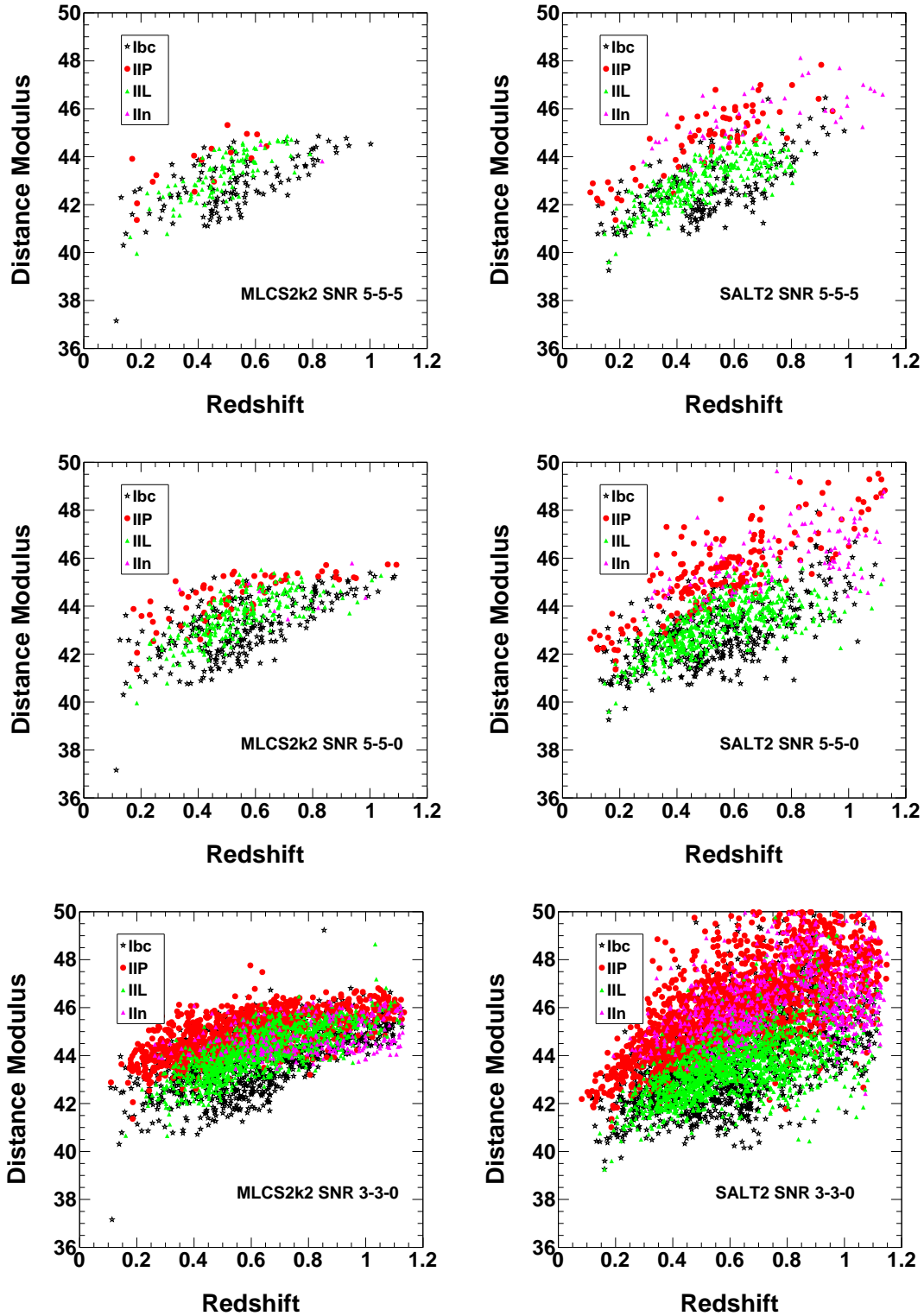


Figure 8. The Hubble scatter is shown for the SNcc sample passing various SNR cuts and a fit probability > 0.1 cut in each case. The left panels are fit with the MLCS2k2 model and the right panels are fit with the SALT2 model.

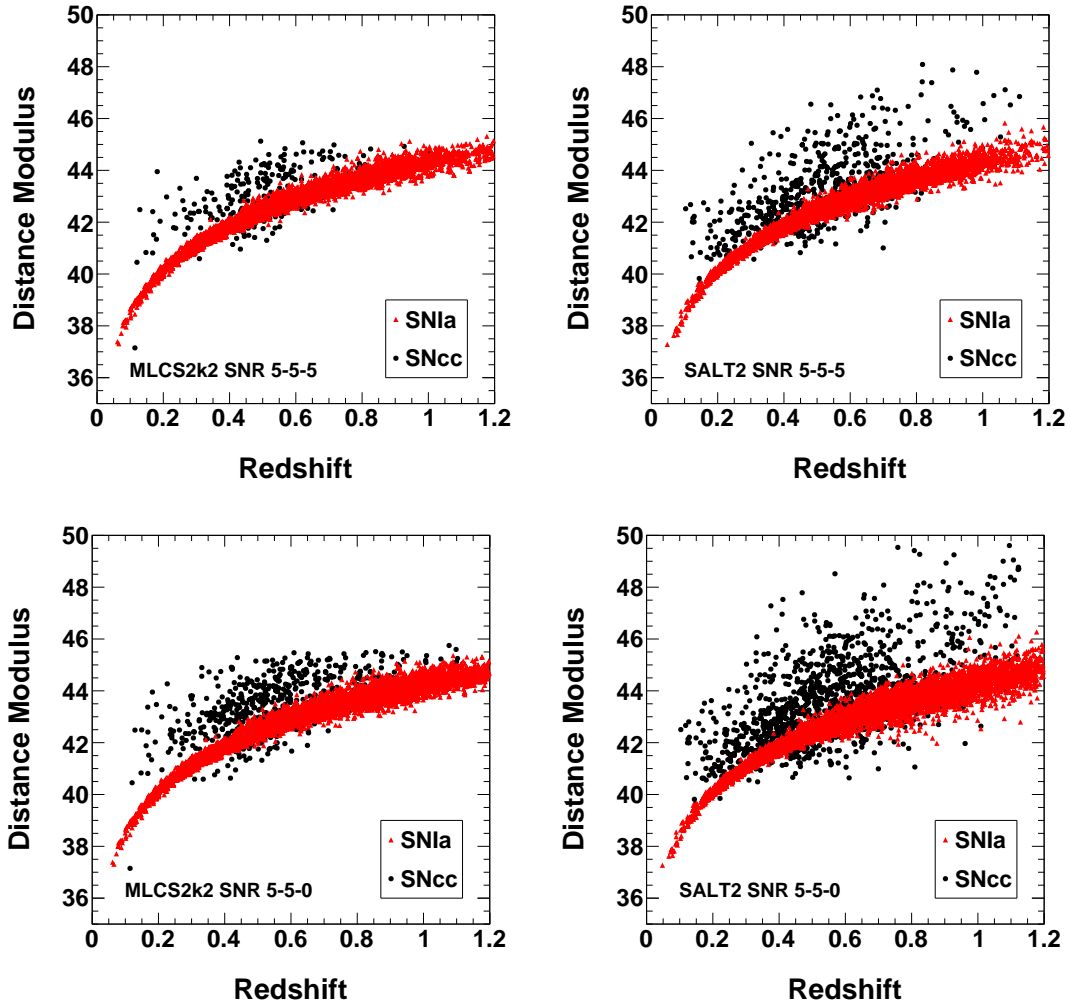


Figure 9. As in Fig. 5, we display four Hubble diagrams, for both SNIa and SNcc. The top panels are for the SNR-5-5-5 cuts, while the lower panels are for the SNR-5-5-0 cuts. The left panels are with the MLCS2k2 light-curve fitter, while the right panels are for the SALT2 light-curve fitter.

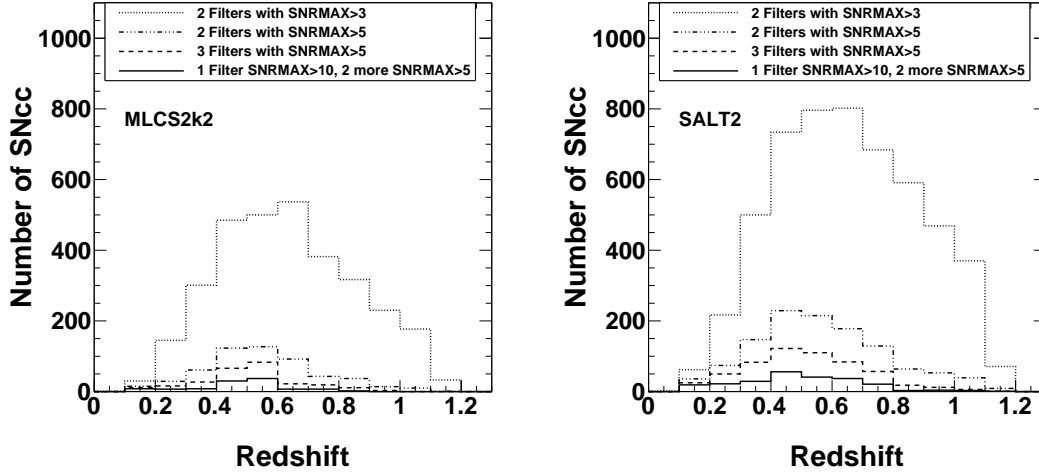


Figure 10. As in Fig. 3, we display redshift distributions for each SNRMAX cut and a fit probability > 0.1 cut, this time for the core collapse samples (fit with MLCS2k2 on the left and fit with SALT2 on the right).

References

- [1] J. P. Bernstein *et al.*, *Supernova Simulations and Strategies For the Dark Energy Survey*, *ArXiv e-prints* (Nov., 2011) [[arXiv:1111.1969](#)].
- [2] P. A. Abell *et al.*, *LSS Science Book, Version 2.0*, *ArXiv e-prints* (Dec., 2009) [[arXiv:0912.0201](#)].
- [3] A. G. Riess *et al.*, *Observational Evidence from Supernovae for an Accelerating Universe and a Cosmological Constant*, *AJ* **116** (Sept., 1998) 1009–1038, [[astro-ph/9805201](#)].
- [4] S. Perlmutter *et al.*, *Measurements of Omega and Lambda from 42 High-Redshift Supernovae*, *ApJ* **517** (June, 1999) 565–586, [[astro-ph/9812133](#)].
- [5] R. Kessler *et al.*, *Results from the Supernova Photometric Classification Challenge*, *PASP* **122** (Dec., 2010) 1415–1431, [[arXiv:1008.1024](#)].
- [6] S. Jha, A. G. Riess, and R. P. Kirshner, *Improved Distances to Type Ia Supernovae with Multicolor Light-Curve Shapes: MLCS2k2*, *ApJ* **659** (Apr., 2007) 122–148, [[astro-ph/0612666](#)].
- [7] J. Marriner *et al.*, *A More General Model for the Intrinsic Scatter in Type Ia Supernova Distance Moduli*, *ApJ* **740** (Oct., 2011) 72, [[arXiv:1107.4631](#)].
- [8] A. Albrecht *et al.*, *Report of the Dark Energy Task Force*, *e-prints arXiv:0609591* (Sept., 2006) [[astro-ph/0609591](#)].
- [9] R. Kessler *et al.*, *SNANA: A Public Software Package for Supernova Analysis*, *PASP* **121** (Sept., 2009) 1028–1035, [[arXiv:0908.4280](#)].
- [10] W. Li *et al.*, *Nearby supernova rates from the Lick Observatory Supernova Search - II*.

- The observed luminosity functions and fractions of supernovae in a complete sample*, *MNRAS* **412** (Apr., 2011) 1441–1472, [[arXiv:1006.4612](#)].
- [11] S. J. Smartt *et. al.*, *The death of massive stars - I. Observational constraints on the progenitors of Type II-P supernovae*, *MNRAS* **395** (May, 2009) 1409–1437, [[arXiv:0809.0403](#)].
- [12] D. Richardson *et. al.*, *A Comparative Study of the Absolute Magnitude Distributions of Supernovae*, *AJ* **123** (Feb., 2002) 745–752, [[astro-ph/0112051](#)].
- [13] M. Chevallier and D. Polarski, *Accelerating Universes with Scaling Dark Matter*, *International Journal of Modern Physics D* **10** (2001) 213–223, [[astro-ph/0009008](#)].
- [14] E. V. Linder, *Exploring the Expansion History of the Universe*, *Physical Review Letters* **90** (Mar., 2003) 091301, [[astro-ph/0208512](#)].